Temperature Accelerated Dynamics in Glass-Forming Materials

Dimitrios G. Tsalikis,[†] Nikolaos Lempesis,[†] Georgios C. Boulougouris,*[,†,‡,§,||] and Doros N. Theodorou*[,†]

School of Chemical Engineering, National Technical University of Athens, Zografou Campus, GR-15780 Athens, Greece, Engineering Informatics and Telecommunications, University of Western Macedonia, Konstantinou Karamanli 55, GR-50100 Kozani, Greece, Department of Chemical Engineering, University of Patras, GR-26500 Patras, Greece, and Scienomics SARL, 17, Square Edouard VII, 75009 Paris

Received: September 16, 2009; Revised Manuscript Received: April 30, 2010

In this work we propose a methodology for improving dynamical sampling in molecular simulations via temperature acceleration. The proposed approach combines the novel methods of Voter for temperature-accelerated dynamics with the multiple histogram reweighting method of Ferrenberg and Swendsen, its dynamical extension by Nieto-Draghi et al., and with hazard plot analysis, allowing optimal sampling with small computational cost over time scales inaccessible to classical molecular dynamics simulations by utilizing the "inherent structure" idea. The time evolution of the system is viewed as a succession of transitions between "basins" in its potential energy landscape, each basin containing a local minimum of the energy (inherent structure). Applying the proposed algorithm to a glass-forming material consisting of a mixture of spherical atoms interacting via Lennard-Jones potentials, we show that it is possible to perform an exhaustive search and evaluate rate constants for basin-to-basin transitions that cover several orders of magnitude on the time scale, far beyond the abilities of any competitive dynamical study, revealing an extreme ruggedness of the potential energy landscape in the vicinity of the glass transition temperature. By analyzing the network of inherent structures, we find that there are characteristic distances and rate constants related to the dynamical entrapment of the system in a neighborhood of basins (a metabasin), whereas evidence to support a random energy model is provided. The multidimensional configurational space displays a self-similar character depicted by a fractal dimension around 2.7 ($\pm$0.5) for the set of sampled inherent structures. Only transitions with small Euclidean measure can be considered as localized.

Introduction

Over the last decades, molecular simulation has been used in a variety of applications in order to predict macroscopic properties of matter based on interatomic interactions, providing a link between the atomistic "picture" and the macroscopically observed thermodynamic and dynamical properties. An important role in the expansion of molecular simulation has been played by the exponential growth of the computational capabilities available to the scientific community, as depicted by Moore's law.[1] At least as important, however, has been the contribution of several methodological and algorithmic developments that made molecular simulation applicable to more and more complex systems. Interestingly, the two originally proposed approaches to molecular simulation, molecular dynamics (MD)[2] and Monte Carlo (MC),[3] still continue to flourish side by side.

On one hand, MC has enabled us to use the complete arsenal of equilibrium statistical mechanics, e.g., perform sampling in all sorts of ensembles, a spectacular example being the Gibbs ensemble[4] that allowed the simulation of phase equilibria without the presence of an interface. Furthermore, MC offers the ability to perform unnatural moves that allow the equilibration of, e.g., polymeric molecules in realistic simulation time.[5]

On the other hand, MD allows the evaluation not only of thermodynamic, but also of dynamical properties at, and away from, equilibrium. As in the case of MC, MD has been implemented in a variety of ensembles that, through the approach of Nosé-Hoover,[6] can be linked to the microcanonical ensemble within the framework of Gibbs statistics. Again the development of methods such as constraint MD[7] and multiple time step algorithms[8] gave a great push, enabling longer and longer time simulations. Furthermore, MD is the natural choice for addressing nonequilibrium phenomena (see, for example, the recent series of nonequilibrium theories, such as the fluctuation theorems[9] or the Jazynski equality,[10] which relate properly selected ensembles of molecular trajectories with the second law of thermodynamics and quantities such as the rate of entropy production, work, and heat exchange).[11]

Another difference between the evaluation of thermodynamic and dynamical properties is the ability of performing independent parallel computations. The computation of any thermodynamic property can trivially be decomposed as the average of independent runs, provided that the equilibration of a single run is not a rate-limiting step. For dynamics, the case is not as trivial. While conducting MD simulations in parallel for different parts of a very large system through spatial domain decomposition is practiced routinely, parallelizing along the dimension of time is much more subtle. In most cases, the parallel decomposition of time will not produce independent runs, resulting in limitations to the parallel efficiency. One shining counterexample is

* Author to whom correspondence should be addressed. Fax +30 210 772 3112. E-mail: doros@central.ntua.gr (D.N.T.); gboul@chemeng.upatras.gr (G.C.B.).
[†] National Technical University of Athens.
[‡] University of Western Macedonia.
[§] University of Patras.
[||] Scienomics SARL.

10.1021/jp908975d
Published on Web 05/21/2010

the work of Voter,[12–14] where, under the assumption of Poisson statistics for infrequent event processes, the dynamical evolution of the system is decomposed into "nearly" independent runs. Furthermore, in limited cases, the dynamics can even be accelerated[12–17] via a biased sampling, as in MC.

Theory

In this work, we propose a methodology for the improvement of dynamical sampling via temperature acceleration. The proposed approach combines the novel methods of Voter of temperature-accelerating dynamics[12–14] with the multiple histogram reweighting method of Ferrenberg and Swendsen,[18] the dynamical extension of this method by Nieto-Draghi et al.,[15] and hazard plot analysis.[19,20] It has been especially designed to address sampling difficulties in atomistic simulations of glass-forming materials in the vicinity of the glass transition temperature T_g. In general, the proposed method can be applied with minimal modification to a variety of systems, provided that the overall dynamics of the systems can be decomposed into slow and fast processes, with the slow processes comprising a Poisson process. In the specific case of glass forming materials, this separation of time scales is provided via the idea of inherent structures (ISs).[21] An IS is the configuration at a local minimum of the potential energy. Glassy dynamics, well below the glass transition temperature T_g, is envisioned as a combination of two types of motions: (a) an "in basin" vibrational motion in the vicinity of a local minimum of the potential energy, and (b) transitions from one basin to another. In the vicinity of T_g, the basin-to-basin transitions are no longer rate-limiting. Instead, transitions from collections of fast-communicating basins, characterized as metabasins (MBs), to neighboring MBs are.[22]

The proposed methodology is highly parallelizable and allows the temperature acceleration of the dynamics upon the assumption of Poisson statistics by histogram reweighting of appropriately constructed ensembles of trajectories. Thereby, the flux in configuration space toward neighboring MBs can be sampled at small computational cost over time scales inaccessible to the classical molecular simulations. Our approach has been developed in order to address some of the main obstacles in the study of glassy materials via molecular simulation.

Over the years, glass-forming materials have been categorized according to various criteria: (A) based on the temperature dependence of dynamic viscosity,[23] into strong and fragile glass-forming liquids, and (B) based on the intramolecular interactions responsible for dynamical entrapment,[24] into repulsive and attractive glasses. Repulsive glasses are usually observed at high densities, where repulsive interactions become dominant, whereas attractive glasses appear as a result of a strong short-range attractive interaction.[25] On the other hand, glasses are systems whose potential energy landscape can be seen to consist of basins separated by high energy barriers, and the long time dynamics can be expressed[21,26–30] by tracing the transitions from one basin to the other.[31–34]

Recently we have shown that it is possible to reconstruct the full dynamics of an atomistic model glass at temperatures well below T_g based on the idea of ISs by combining the fast "vibrations" within a basin around the IS and the slow transitions from one basin to another.[32] For temperatures above T_g, on the other hand, the long time diffusion can be described accurately simply through the mean square displacement of atoms accompanying transitions from one potential energy minimum to another.[32]

A decisive step in these calculations is the evaluation of the rate constants for the elementary transitions between basins. For this evaluation, one can use a variety of methods, from saddle point calculations[35–38] to transition path sampling.[39–41] Due to the dramatic change in the spectrum of times characterizing the glass-forming system as the temperature changes by only a few percent of T_g through the glass transition, a single simulation method is not expected to provide optimal conditions both above and below T_g. As one would expect, at very low temperatures, saddle point calculations can be very efficient.[33,34] For temperatures far above T_g, brute force MD is clearly the optimal choice, whereas, for conditions close to T_g, none of the above is expected to be numerically efficient. In recent work[42] we have shown that an appropriate ensemble of short MD trajectories can be generated in parallel and can thus make the evaluation of the rate constants in the vicinity of T_g feasible. In this work we show how it is possible to accelerate the dynamical sampling of the interbasin transitions and rate constants, allowing MD to sample several orders of magnitude on the time scale with minimal computational overhead.

The heart of the rate calculation is based on "hazard plot"[19,20] analysis of the atomistic MD trajectory. Hazard plot analysis not only provides the rate constant, but can also be used to test the validity of the Poisson approximation for the actual process. The rate constant λ is typically evaluated as the slope of the cumulative hazard $H(t) = \int_0^t h(t')\,dt'$. Here, $h(t)$ is the hazard rate, defined such that $h(t)\,dt$ is the probability that a system, which has survived a time t since its last transition, will undergo a transition at the time between t and $t+dt$. For a Poisson process with rate constant λ, the hazard rate is independent of time, $h(t) = \lambda$. The cumulative hazard is $H(t) = \lambda t$, and the probability that a transition occurs in a time less than t since the last transition is $P(t) = 1 - \exp[-\lambda t]$. Therefore, the rate constant can be evaluated as the slope of $-\ln(1 - P(t))$ with respect to time.

Once the rate constants are known for transitions leading out of a specific part of the potential energy landscape with first-order kinetics, then the dynamical evolution of the system can be efficiently sampled via the dynamical integration over a Markovian web (DIMW) methodology developed by Boulougouris and Theodorou.[34] DIMW is an alternative to kinetic MC sampling, which enables the direct evaluation of the time-dependent probability of occupancy of states (here, basins) for a system undergoing successive transitions with first-order kinetics between states in a landscape of infinite extent. On the basis of DIMW, it is possible to construct an ever-expanding network of known or "explored" states, bounded by a set of "boundary" states, starting from an initial (small) set of states. For each explored state, all relevant transitions connecting it with its neighboring states have been located, and the corresponding transition rate constants computed by atomistic infrequent-event analysis. Boundary states are connected to explored states, but are not yet explored themselves. The time-dependent probability distribution among explored states is determined via analytical solution of the master equation for the "explored" states under absorbing boundary conditions for the "boundary" states. The set of explored states is expanded systematically whenever necessary, through a stochastic scheme that each time selects to include in the set of explored states a boundary state, according to the probability flux to that state. DIMW only requires an "on the fly" evaluation of the rate constants in order to reproduce the full dynamics of the system in an analytical form. This form allows the use of the EROPHILE formalism,[33] which provides a dual geometric representation of relaxation modes: (a) a mode that corresponds to a perturbation from the equilibrium probability distribution

among states that decays with time along a single exponential, and, most importantly, (b) a mode that is identified with a linear combination of observables that, upon *any* perturbation from equilibrium, will return to equilibrium in a single exponentially decaying fashion.

In the literature, there are several approaches to the estimation of rate constants that are more rigorous and exact compared to the proposed approach. Nevertheless, we have shown[31,32] that the hazard plot-based methodology for evaluation of the rate constant proposed in this work is sufficient to reproduce the dynamics of interbasin transitions in glass-forming systems. A rigorous way of calculating transition rates of rare events is provided by transition path sampling.[40,43,44] This algorithm does not require any prior knowledge of the transition states or of the reaction mechanism. Transition path sampling is based on the earlier ideas of Pratt,[43] in which an MC method was used to find the reaction paths.[17]

The rates for transitions between basins depend strongly on the temperature. If we raise the temperature, all transitions will occur in shorter times, in comparison to the lower temperature, and the dynamics of the system will accelerate. Raising the temperature not only changes the rate constants, but also their relative ratios; therefore the kinetics of the system might be very different at different temperatures. Voter et al. introduced the novel method of temperature-accelerated dynamics (TAD)[12–14] in order to accelerate the system dynamics by raising the temperature and still obtain the correct dynamics. The idea is to use an MD simulation at a higher temperature to find transition pathways and simultaneously generate correctly distributed waiting times at the original temperature. The correction for the bias induced by raising the temperature is based on reweighting of the observed transitions, and allowing only those transitions that would occur at the original temperature. In some cases where the total number of paths is known, it is possible to do a formal reweighting of all possible paths.[17]

In their attempt to combine accelerated dynamics with free-energy calculations in the study of rare events, Tuckerman and co-workers[16,45] developed a method that is based on the creation of an adiabatic separation between the reaction coordinate and the remaining degrees of freedom within an MD simulation. In addition, the reaction coordinate is maintained at a high temperature relative to the remaining degrees of freedom. In this way, the full configuration space corresponding to the rare event is sampled, and the free energy profile is rigorously generated directly from the probability distribution of the reaction coordinate. This method requires no postprocessing of the data and leads to a scheme that is more efficient than methods of constraining (or restraining) the reactive degrees of freedom.

On the other hand, there are several very powerful tools in the study of equilibrium thermodynamics, with very low computational cost, whose potential has not been fully tapped in dynamical simulations. Such tools are the multiple histogram reweighting method introduced by Ferrenberg and Swendsen[18] and the parallel tempering[46] method. At this point, we will briefly describe the multiple histogram reweighting method introduced by Ferrenberg and Swendsen,[18] since it plays a vital role in the proposed methodology.

The utility of histograms stems from their rigorous connection to statistical mechanics, and the ability to extract from them fundamental thermodynamic potentials, which can be used to predict properties of the system under conditions other than those of the original simulation. Multiple histogram reweighting is a tool of particular importance for free energy calculations in barrier crossing problems, e.g., the computation of the free energy barrier between two states (phases, conformations) or the computation of the free energy of systems that cannot be equilibrated by conventional MC or MD simulations due to the complexity of their free energy landscape. The approach of Ferrenberg and Swendsen[18] is based on the idea that it is possible to construct a self-consistent estimate for the histograms without assuming any specific functional form. Whereas in the original work the method was derived based on the potential energy, it is trivial to use the total energy instead, as we do use in our simulations.

The connection between histogram measurements and statistical mechanics lies in the evaluation of the macrostate probability distribution, a macrostate here denoting a set of configurations with the same energy level E. The canonical ensemble yields for the probability of observing the system at a total energy E at given temperature T:

$$p(E,N,V,T) = \frac{\Omega(N,V,E)\mathrm{e}^{-\beta E}}{Z(N,V,T)} \tag{1}$$

where $\Omega(N,V,E)$ is the density of states. The quantity $\Omega(N,V,E)\,\mathrm{d}E$ is equal to the number of states of the N particle system at volume V with total energy between E and $E + \mathrm{d}E$. Z, on the other hand, is the partition function

$$Z(N,V,T) = \frac{1}{N!}\int \mathrm{e}^{-\beta E(\mathbf{r}^N,\mathbf{p}^N)} d^{3N}r d^{3N}p = \int \Omega(N,V,E)\mathrm{e}^{-\beta E}\,\mathrm{d}E$$

.

For the sake of simplicity, as long as we work in the canonical ensemble, we will drop the dependence on the volume (V) and the number of particles (N). Since the partition function is expressed as a sum over macrostates of the system, whose individual terms are proportional to the probability of observing those states during the simulation, the connection between histogram measurements and statistical mechanics becomes trivial. Histograms measure the frequency with which macrostates are sampled, providing an estimate for the corresponding probabilities:

$$p^{\mathrm{hist}}(E,T)\Delta E = \frac{H(E,T)}{M(T)} \tag{2}$$

where $H(E,T)$ is the number of times that the system was observed within the energy range $[E, E + \Delta E)$ at a specific temperature T, and $M(T)$ is the total number of all measurements at this temperature. Let us consider that we have a set of histograms $p_i^{\mathrm{hist}}(E,T_i)$. To obtain the optimal distribution at temperature T_0, Ferrenberg and Swendsen proposed to linearly combine the estimates of all runs using the weighting factor w_i:

$$p^{\mathrm{est}}(E,T_0) = \sum_{i=1}^{n} w_i(E)\exp[-(\beta_0 - \beta_i)E]\frac{Z_i}{Z_0}p^{\mathrm{est}}(E,T_i) \tag{3}$$

where $\beta_0 = 1/(k_{\mathrm{B}}T_0)$ and $w_i(E)$ is a weight function that depends on the energy and the run number, normalized such that the total contribution to $p^{\mathrm{est}}(E,T_0)$ from each run at a given E is equal to one: $\sum_{i=1}^{n} w_i(E) = 1$. The values of the weighting function w_i will be determined in such a way that the variance in the estimated values of the distribution $p^{\mathrm{est}}(E,T_0)$ is minimized. Using the fact that fluctuations in different simulations are uncorrelated, along with standard error propagation rules, we can predict the expected variance in the composite $p^{\mathrm{est}}(E,T_0)$ at

the desired temperature T_0. We minimize this error by optimizing the weight functions $w_i(E)$, using Lagrange multipliers to ensure normalization of $w_i(E)$, resulting in the following form for the measured distribution $p^{\text{est}}(E,T_0)$:

$$p^{\text{est}}(E,T_0) = \frac{\sum_{i=1}^{n} H_i(E) \exp(-\beta_0 E)}{\sum_{i=1}^{n} \exp(-\beta_i E) M_i Z_0 / Z_i} \tag{4}$$

where $H_i(E)$ equals $H(E,T_i)$, M_i equals $M(T_i)$, and Z_i is evaluated by

$$Z_i = \sum_E \mathrm{e}^{-(\beta_i-\beta_0)E} \frac{\sum_{j=1}^{n} H_j(E)}{\sum_{j=1}^{n} \mathrm{e}^{-(\beta_j-\beta_0)E} \frac{M_j}{Z_j}} \tag{5}$$

.

The values for Z_i are calculated self-consistently. Equation 5 has to be solved iteratively to find the Z_i's as functions of one reference, e.g., Z_0. The initial values are taken to be $Z_i = 1$. Then the Z_i are re-evaluated via eq 5. This iterative process proceeds until converged values are obtained from eq 5. Actually, it is only possible to determine relative values for the Z_i, and the corresponding free energies, using these equations. Typically one run is chosen to be the reference state, for which Z_i is always set to unity. Obtaining the set of Z_i, one can recover the $p^{\text{est}}(E,T_0)$, for any temperature T_0 in the range between T_1 and T_n, for which we collected our histograms.

Subsequently, one can recover the average value for any order parameter Q that has been reweighted for a series of temperatures:

$$\langle Q \rangle_{T_0} = \frac{\int Q(E) p^{\text{est}}(E,T_0)\, \mathrm{d}E}{\int p^{\text{est}}(E,T_0)\, \mathrm{d}E} \tag{6}$$

The reader will find a generalized description of the multiple histogram reweighting method in the book of Frenkel and Smit.[47]

The multiple histogram reweighting method has been widely used for the determination of thermodynamic equilibrium properties from a reduced amount of MC data. Nieto-Draghi et al.[15] showed that this method is applicable to dynamical properties obtained from MD simulations. This application is based on the idea that the canonical ensemble average can be expressed as an ensemble average over microcanonical trajectories weighted with the corresponding canonical probability distribution. The results obtained showed that their application is suitable for the evaluation of correlation functions, as well as for the determination of transport coefficients through Green−Kubo and Einstein relations.

In this work we combine the above methodologies in order to derive a method for the temperature acceleration of an ensemble of trajectories leading from one part of the potential energy landscape to another. We consider a simulation in the canonical ensemble (*NVT*), under constant temperature T_0, during which we observe the transitions between potential energy minima. If we assume that the interactions between the thermostat and the system are weak, so that, in the limit of time required for a transition, no energy exchange between the thermostat and the system takes place, then equivalently we can consider that every transition is performed under constant total energy. In recent work we have tested this assumption, and we have also shown that, by considering an ensemble average of *NVE* trajectories initiated from configurations weighted according to the canonical destribution, we can efficiently parallelize the computation of the residence time in the vicinity of potential energy minima in glassy systems.[42]

In this work we will show how to use the multiple histogram method in order to combine trajectories generated at different temperatures and thereby create an appropriately weighted ensemble of trajectories that incorporate the observed transitions and provide access to a wide range of time scales for each temperature. Once we have created such an ensemble, we know from hazard plot analysis[19,20] that the transition rate out of a selected minimum of the potential energy can be determined by the long-time behavior of the cumulative probability $P(t)$ versus the residence time t. As we have shown[42] (compare eq 6), an estimate of the cumulative probability $\hat{P}^{\alpha}_{NVT_0}(t)$ that a transition of specific type (from a given origin state α to all possible neighboring destination states β) will take place in a time less than or equal to t since the last entry to state α at temperature T_0, can be obtained as

$$\hat{P}^{\alpha}_{NVT_0}(t) = \frac{\int \hat{P}^{\alpha}_{NVE}(t) p^{\text{est}}(E,T_0)\, \mathrm{d}E}{\int p^{\text{est}}(E,T_0)\, \mathrm{d}E} \tag{7}$$

where $\int p^{\text{est}}(E,T_0)\, \mathrm{d}E = 1$. In eq 7, as in eqs 3 and 4, $p^{\text{est}}(E,T_0)$ is an estimate of the probability of encountering the system with energy E at temperature T_0. The term $\hat{P}^{\alpha}_{NVE}(t)$ is the cumulative probability that a transition from state α to any neighboring state will take place in time $\leq t$ since the last entry to state α at energy E. $\hat{P}^{\alpha}_{NVE}(t)$ is a function of E; it will be determined by hazard plot analysis, by grouping the transitions observed at the same constant energy E out of each basin of the studied MB.[42] Equation 7 enables a reduction of the canonical ensemble dynamical behavior to an ensemble average over Boltzmann weighted microcanonical ensemble trajectories. We use it to evaluate $\hat{P}^{\alpha}_{NVT_0}(t)$ via histogram reweighting, based on simulations carried out at $T > T_0$. For each one of the temperatures used in the multiple histogram method, we gather two pieces of information in order to compute eq 7: (A) the number $H(E,T)$ of times that the system was observed within the range $[E, E + \Delta E)$ at a specific temperature T, in order to evaluate $p^{\text{est}}(E,T_0)$ from eqs 4 and 5, and (B) the cumulative probability functions of residence times $\hat{P}^{\alpha}_{NVE}(t)$ over the range of E such that $H(E,T) \neq 0$. The final $\hat{P}^{\alpha}_{NVE}(t)$ is formed by combining all measurements at the energy level E, no matter which temperature they came from. As we have argued in our recent work,[42] describing the ensemble average of trajectories of an *NVT* ensemble via a properly weighted ensemble of *NVE* trajectories corresponds to a superposition ansatz for the residence time distribution. Given eq 7, the sum of rate constants for leaving state α at temperature T_0 can be evaluated from the long-time slope of $-\ln(1 - \hat{P}^{\alpha}_{NVT_0}(t))$ with respect to t.[42]

As we have shown,[31] for any Poisson process we can calculate the individual transition rates from state α toward its neighboring states β, by evaluating the conditional probability $\Pi^{NVT_0}_{\alpha\to\beta}$ to undergo a transition from α to β, provided we are moving out of α. The probability $\Pi^{NVT_0}_{\alpha\to\beta}$ is equal to

$$\Pi^{NVT_0}_{\alpha\to\beta} = \frac{m_\beta}{n_\alpha} \tag{8}$$

where n_α is the number of transitions started from minimum α, and m_β is the number of transitions that started from minimum α and ended in minimum β, all at temperature T_0. We can write

$m_\beta = m_{E1} + m_{E2} + ... + m_{E_m}$ where m_{E_i} is the number of times we observed a transition from α to β under constant energy E_i.

$$\Pi_{\alpha\to\beta}^{NVT_0} = \frac{m_\beta}{n_a} = \frac{m_{E_1} + m_{E_2} + ... + m_{E_m}}{n_a} = \frac{m_{E_1}}{n_a} + \frac{m_{E_2}}{n_a} + ... + \frac{m_{E_m}}{n_a} \quad (9)$$

Let u_{E_i} be the total number of transitions (toward any state neighboring α) that were observed under constant energy E_i. Then eq 9 gives:

$$\Pi_{\alpha\to\beta}^{NVT_0} = \frac{m_{E_1}}{n_a}\frac{u_{E_1}}{u_{E_1}} + \frac{m_{E_2}}{n_a}\frac{u_{E_2}}{u_{E_2}} + ... + \frac{m_{E_m}}{n_a}\frac{u_{E_m}}{u_{E_m}} = \frac{m_{E_1}}{u_{E_1}}\frac{u_{E_1}}{n_a} + \frac{m_{E_2}}{u_{E_2}}\frac{u_{E_2}}{n_a} + ... + \frac{m_{E_m}}{u_{E_m}}\frac{u_{E_m}}{n_a} \quad (10)$$

As in the derivation[42] of eq 7, we can replace $(u_{E_i})/(n_a)$ with $p(E_i,T_0)$:

$$\Pi_{\alpha\to\beta}^{NVT_0} = \frac{m_{E_1}}{u_{E_1}}p(E_1,T_0) + \frac{m_{E_2}}{u_{E_2}}p(E_2,T_0) + ... + \frac{m_{E_m}}{u_{E_m}}p(E_m,T_0) \quad (11)$$

The quantity m_{E_i}/u_{E_i} corresponds to the conditional probability that a transition out of α will lead to β in a simulation performed in the microcanonical ensemble under constant energy E_i, $\Pi_{\alpha\to\beta}^{NVE_i}$. We rewrite eq 11 as

$$\Pi_{\alpha\to\beta}^{NVT_0} = \Pi_{\alpha\to\beta}^{NVE_1}p(E_1,T_0) + \Pi_{\alpha\to\beta}^{NVE_2}p(E_2,T_0) + ... + \Pi_{\alpha\to\beta}^{NVE_m}p(E_m,T_0) \to \Pi_{\alpha\to\beta}^{NVT_0} = \frac{\int \Pi_{\alpha\to\beta}^{NVE}p^{\mathrm{est}}(E,T_0)\,\mathrm{d}E}{\int p^{\mathrm{est}}(E,T_0)\,\mathrm{d}E} \quad (12)$$

Similarly to eq 7, eq 12, which is again of the form of eq 6, relates the dynamical behavior of the canonical ensemble to an ensemble average of Boltzmann-weighted microcanonical trajectories. The quantity $\Pi_{\alpha\to\beta}^{NVE}$ will be determined using our parallel methodology and in this case is combined from all the measurements at the energy level E, sampled at all temperatures where $H(E,T) \neq 0$. It measures the fraction of transitions starting from α that have been observed to end up in β at the energy level E. In Figure 1, we summarize all the steps for the implementation of the temperature acceleration method. It is trivial to see that the swarm of microcanonical trajectories whereby the probabilities $\Pi_{\alpha\to\beta}^{NVE}$ are computed can be parallelized efficiently based on our recently proposed scheme.[42]

As in our previous work,[34] the MD simulations required for accumulating $\hat{P}_{NVE}^{\alpha}(t)$ and $\Pi_{\alpha\to\beta}^{NVE}$ are conducted in parallel, as a swarm of independent "branch" *NVE* trajectories initiated at phase-space points sampled at regular intervals along an *NVT* "backbone" trajectory, which is artificially trapped inside an MB.[42] The entrapment of the system is achieved by inversion of the momenta, once the system exits the MB, stepping the system backward, returning it to the MB. The procedure has been described in our previous work. The inversion of momenta is followed by an appropriate "thermalization." A Gaussian randomization (that preserves the canonical distribution) of the momenta is used in order to perturb the system from the original trajectory and assist the chaotic character of the system dynamics in sampling nearby trajectories. In general, the procedure introduced in our recent work[42] allows the automated definition of a MB based on the sampling abilities of the MD simulation

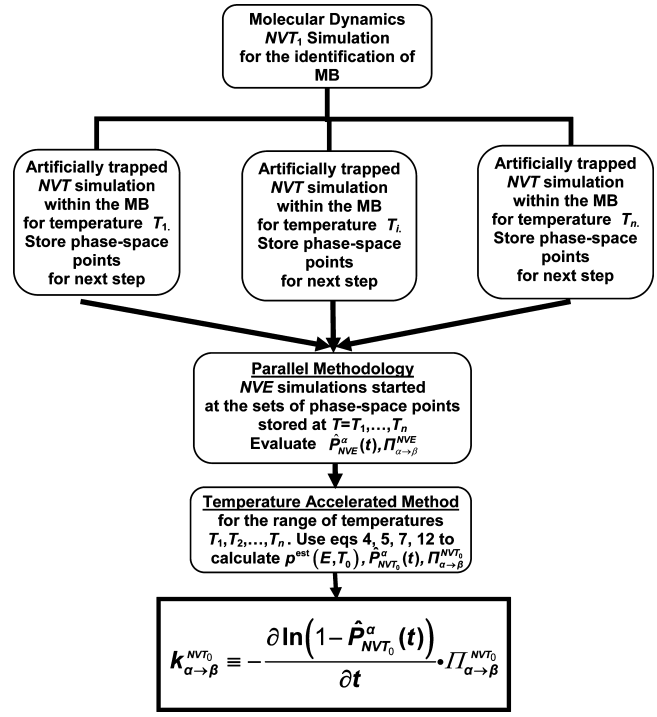

Figure 1. Representation of the temperature-accelerated method.

under the given conditions.[42] To check whether a given configuration is in a given explored MB, we minimize its energy and examine whether the configuration and energy of the minimum coincide, within numerical accuracy, with those of one of the ISs assigned to the MB.

Prior to our automated definition of a MB based on the rate of exploring new basins,[42] there have been several significant attempts to define MBs.[48–52] A good source of information on the subject is the recent review by Heuer.[53]

Going beyond that work, however, we here generate backbone *NVT* trajectories over a wide range of temperatures T_i and reweight the energy histograms of these trajectories to obtain $p^{\mathrm{est}}(E,T_0)$ at the temperature of interest, T_0, according to eqs 4 and 5. All branch trajectories at energy level E, irrespective of the temperature of the backbone trajectory off of which they were generated, are taken into account in accumulating $\hat{P}_{NVE}^{\alpha}(t)$ and $\Pi_{\alpha\to\beta}^{NVE}$. This is done for all E values accessed by our simulations. The rate constant $k_{\alpha\to\beta}^{NVT_0}$ connecting state α to state β may be obtained for any temperature T_0 within the range of the simulation temperatures used in the multiple histogram schemes as the product of $\Pi_{\alpha\to\beta}^{NVT_0}$ and the slope of $-\ln(1 - \hat{P}_{NVT_0}^{\alpha}(t))$ with respect to time. Here, $\Pi_{\alpha\to\beta}^{NVT_0}$ and $\hat{P}_{NVT_0}^{\alpha}(t)$ are evaluated from $\Pi_{\alpha\to\beta}^{NVE}$, $\hat{P}_{NVE}^{\alpha}(t)$, and $p^{\mathrm{est}}(E,T_0)$ computed for the various E values based on eqs 7, 12, and 4.

In Figure 1 we summarize all the steps for the implementation of the temperature acceleration method.

Results and Discussion

It has been shown that the dynamics of a glassy material can be described by mapping onto a sequence of transitions between basins, each basin constructed around an IS.[32] The system chosen in this work to model glass-forming materials is a popular two-component mixture of Lennard-Jones spheres initially proposed by Kob et al.[54] The atomic fractions of A and B are 80.03% and 19.97%, respectively, and the total number of particles is 641 (513 A's and 128 B's). A and B atoms are of equal mass ($m_A = m_B = 6.634 \times 10^{-26}$ kg) but differ in their interactions.

The system has been especially designed to avoid crystallization and is widely used as a model for glass-forming materials.[31,32,54–59] The Lennard-Jones interaction parameters are $\varepsilon_{AA} = 1.65678 \times 10^{-21}$ J, $\sigma_{AA} = 3.4 \times 10^{-10}$ m, $\varepsilon_{BB} = 0.82839 \times 10^{-21}$ J, $\sigma_{BB} = 2.992 \times 10^{-10}$ m, $\varepsilon_{AB} = 2.48517 \times 10^{-21}$ J, and $\sigma_{AB} = 2.72 \times 10^{-10}$ m. The unit for reducing time is selected[38] as $[m_A\sigma_{AA}^2/(48\ \varepsilon_{AA})]^{1/2} = 3.10 \times 10^{-13}$ s, and the unit for temperature is $\varepsilon_{AA}/k_B = 120$ K. If the above Lennard-Jones interaction parameters are reduced by the values of the A−A interaction parameters, they read[38] $\varepsilon_{AA} = 1.0$, $\sigma_{AA} = 1.0$, $\varepsilon_{BB} = 0.5$, $\sigma_{BB} = 0.88$, $\varepsilon_{AB} = 1.5$, $\sigma_{AB} = 0.8$. In all calculations reported here, the molecular density of the system will be 1.1908 σ_{AA}^{-3}. In the following discussion, properties will be reported in both reduced units (r.u.) and physical units, where appropriate.

For this system, Kob and Andersen[57] have estimated the mode coupling critical temperature T_c to be 0.435 in reduced units (∼52.2 K), whereas the glass transition temperature has been predicted[17] by Shell et al.[59] to be $T_g = 0.32$, that is to say roughly equal to 38.4 K.

In order to confirm the validity of the proposed methodology, we compare rate constants $k_{\alpha\rightarrow\beta}^{NVT_0}$ with the results of our recent work on the autotuned evaluation of transition rates within and out of a MB via an efficient parallel scheme.[42]

More precisely, we compare the transition rate constants $k_{\alpha\rightarrow\beta}^{NVT_0}$ of a selected MB toward its neighboring minima against the results obtained from our single-temperature parallel method[42] at temperature $T_0 = 37$ K. For the proposed temperature-accelerated method, we used data from seven different temperatures, ranging from 37 to 55 K. These temperatures were 37, 40, 43, 46, 49, 52, and 55 K (corresponding to 0.31, 0.33, 0.36, 0.38, 0.41, 0.43, 0.46, in r.u., respectively).

The comparison, presented in Figure 2, shows excellent agreement between our new, temperature-accelerated method and the single-temperature method of ref 42. This check has been performed for all 290 minima in the MB, and the results were also in excellent agreement.[42]

In summary, with the brute force MD at 37 K (0.31 r.u.), simulating for 3 ns (9677 r.u.) we found 3910 connections between the 90 minima in our MD; with the single-temperature parallel scheme (corresponding to 77 ns) we observed 24271 connections, whereas with the temperature acceleration scheme proposed here we collected 51207 connections. In terms of real execution time, with brute force MD we explored ∼325 transitions/CPU hour; with the single-temperature parallel scheme we explored ∼1867 transitions/CPU hour, whereas with the new scheme we quantified ∼3660 transitions/CPU hour within and out of the studied MB. Note that, since the rate of "exploring" new transitions is not linear with respect to the simulation time, the gain from the proposed scheme if far greater than an order of magnitude. The simulations were performed on the IBM BCX/5120 cluster of the Cineca Supercomputer Center in Bologna, Italy, which is mainly used for massively parallel applications and special high-end projects. The cluster consists of 2180 nodes, where each node is supplied with two Opteron Dual Core Processors at 2.6 GHz. The nodes communicate via an infiniband (5Gb/s) network. More information about the cluster can be found at the URL http://www.cineca.it.

In Figure 3, we compare the distribution for the individual transition rates of the MB at 37 K, as identified by (a) an artificially trapped MD simulation, (b) our recently proposed single-temperature parallel method,[42] and (c) by the method of temperature acceleration proposed here. The results in Figure 3 are presented in the form of the number of transitions explored by each of the above approaches binned according to the value

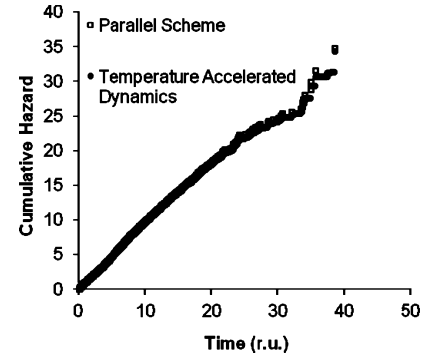

Figure 2. Comparison of the transition rate constant $k_{\alpha\rightarrow}^{NVT_0} = \sum_\beta k_{\alpha\rightarrow\beta}^{NVT_0}$ out of a selected potential energy minimum using the parallel method[42] (□) and the proposed method (—) at the same temperature $T_0 = 37$ K. We observe that the results are in excellent agreement.

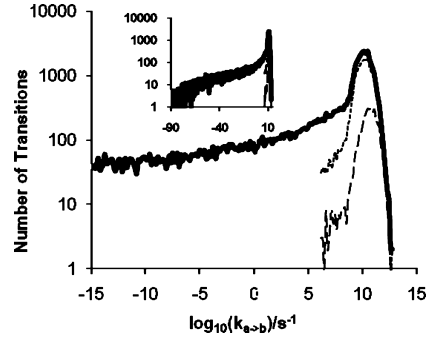

Figure 3. Comparison of the number of identified transitions between the basins of a specific MB at temperature 37 K, classified according to their rate constants, as obtained by different methods: (a) an MD simulation at 37 K (0.31 in r.u.) artificially trapped within the MB (long-dashed line), (b) the single-temperature parallel method at 37 K[42] (dashed line), (c) the proposed temperature-accelerated method, using as input data from method b for a range of temperatures from 37 to 55K, (0.46 in r.u.) (solid line). Inset: the same plot for the total range of rate constants sampled by the temperature-accelerated method.

of the decimal logarithm of the rate constants of the transitions. (The binning interval was set to 0.15, with the rate constant in units of inverse seconds).

It should be noted that the difference between the brute force MD sampling methods (a) and the recently proposed parallel scheme method (b) is strictly related to the total length of the MD trajectories generated. Whereas in the brute force MD (a) we used 12 CPU hours on one processor, in the parallel scheme (b) we utilized ∼250 CPU hours distributed over 250 processors, resulting in approximately the same real execution time. As a consequence, we increased our sampling window by an order of magnitude, observing all the rates that the brute force MD was able to visit plus rates slower by 1 order of magnitude. As we have described in our recent work,[42] the parallel scheme does not accelerate the dynamics but simply allows the distribution of the computational load in a very efficient manner. On the other hand, the temperature acceleration scheme (c) proposed in this work combines seven temperatures and therefore utilizes seven times more CPU time, relative to the single-temperature parallel scheme. However, it provides an exponential acceleration of dynamics, since, as can be seen from Figure 3, it retrieves all transitions found in the parallel scheme, but now it provides sampling of rates over an extremely broad window of time scales. From Figure 3 it is obvious that the temperature-accelerated method (c) can sample transition rates that range over many orders of magnitude. As one can clearly see, the developed methodology can evaluate extremely slow

transition rate constants, more than 20 orders of magnitude slower than conventional MD, that are inaccessible by any classical molecular simulation method. The comparison between those methods makes us confident that we have performed exhaustive sampling in the given part of the landscape, although to our knowledge there is no theoretical way that this can be guaranteed.

The physical information conveyed by Figure 3 and its inset is significant. Two distinctive characteristics of the rate constant spectrum are (a) a very broad "wing" that decays in power law fashion [$\rho(k_{a\to b}/\nu_0) \approx B\ (k_{a\to b}/\nu_0)^{\alpha-1}$ with $\alpha \approx 0.01$] toward extremely low values of $k_{a\to b}$; (b) a "nose" around $k_{a\to b} = 10^{10}$ s^{-1}. The broad, slowly decaying wing is associated with the ruggedness of the potential energy landscape. The nose indicates that the sampled set of transitions has a strong contribution from the range $10^{12}-10^{8}$ s^{-1}. This is a consequence of the way in which the set of basins a and b has been picked. Both a and b have been sampled as basins belonging to the same MB; therefore, they are likely to communicate with each other through facile transitions going over relatively low energy barriers. Indeed, the residence time within the MB explored here is on the order of 10^{-10} s, i.e., right at the time scale corresponding to the tip of the nose of the rate constant spectrum of Figure 3 (compare Figure 1 (inset) and Figure 2 of ref 42, from which an estimate of the mean residence time in the MB can be extracted). Thus, the nose in Figure 3 of the current paper and the kink between the nose and the wing are a consequence of our dynamical sampling scheme. Higher-energy passages among the basins of the MB, which contribute to the wing, are less likely to be biased by the fact that the basins belong to the same MB. Thus, we believe the wing to be a true reflection of the actual distribution of barrier heights in the energy landscape of our glass-forming system.

It should be emphasized that our ability to perform an exhaustive search for transition paths, beyond the capabilities of any known method, can serve as a tool to overcome the irreversible nature of the dynamics in the vicinity of the glass transition temperature within the sampled MBs. Of course, we only present here a test calculation where all transition paths emanate from the basins of an originally defined MB.[42] The system is not going to stay in the specific MB for times long enough for the slow transitions identified here to be observed. Yet, our ability to evaluate these slow transitions provides us with a tool for fully exploring the landscape around any basin. In other words, the use of classical MD would lead us to the observation of irreversible processes, where, for the vast majority of trajectories, only the fastest transitions would be observed, while transitions with inverse rate constants significantly longer than the maximum simulation time would not be sampled at all. The result would be an irreversible dynamical evolution of the system. Using the proposed method, we have the opportunity to calculate both forward and reverse transitions, no matter how slow they are. In this way we can express the irreversible dynamics based on a *reversible* reference process. By coupling this scheme for locating paths and transition rate constants with DIMW,[34] we will be able to observe the very slow hierarchical process of spreading across MBs and meta-MBs as the system seeks to establish thermodynamic equilibrium, and thus explore specimens with macroscopically relevant aging histories.

It is of particular importance that, since we know the transition rate constants from and to any sampled state, our system becomes, by construction, ergodic, if we have the ability to observe it for long times, such that transitions from all to all states would have the chance to occur. It is now possible to examine for which observation times our system, in our chosen set of basins, diverges from ergodicity, an aspect that is of particular importance for the definition of the mode-coupling T_c, the glass transition, and its direct connection with the ISs picture.

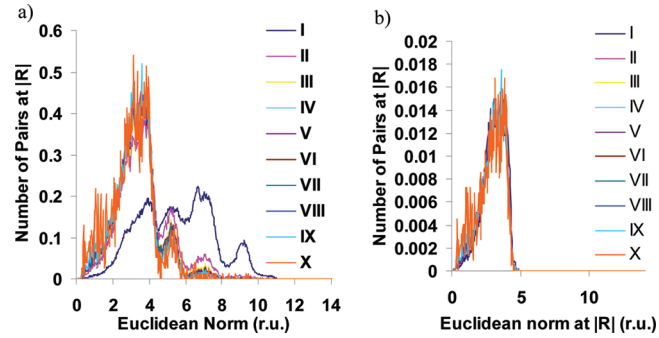

Figure 4. Number of identified transitions between ISs as a function of their Euclidean distance. All distributions are normalized. Results are shown for various upper bounds on the rate constants associated with the transitions, to uncover how the distribution of directly connected basins varies with the time window used to define connectivity. (a) For all ISs, irrespectively of whether they belong to the same MB or not, (b) only for ISs belonging to the same MB. Starting from the top, we plot the numbers of transitions between ISs at a specific Euclidean distance (I) with no restriction with respect to direct connectivity (all-to-all); (II) provided that we found a direct connection with the TAD; (III−XI) provided that we found a direct connection with rate constant k_{ij} faster than 10 s^{-1} for III; faster than 10^3 s^{-1} for IV; faster than 10^5 s^{-1} for V; faster than 10^7 s^{-1} for VI; faster than 10^8 s^{-1} for VII; faster than 10^9 s^{-1} for VIII; faster than 10^{10} s^{-1} for IX; and faster than 10^{11} s^{-1} for X.

In Figures 4 and 5 we analyze the resulting network of interconnecting basins in terms of the length, in the multidimensional Euclidean space of atom positions, spanned by ISs we have identified as belonging either to the studied MB or to one of its first neighbors. In Figure 4 we plot the normalized distribution of identified transitions between neighboring basins against the Euclidean distance between their ISs in configuration space. Results are given for various time windows, corresponding to the inverse rate constants of the direct transitions considered. Note that the Euclidean space is of 3×641 dimensions for our system of 641 particles. In Figure 4a we do not discriminate depending on whether the considered connected ISs belong to the same MB. In Figure 4b, on the other hand, we only consider minima within the same MB. In both figures we illustrate the effect of the existence of direct transitions within a time window specified by the corresponding rate constant, including in the construction of the histogram only minima that are connected with faster rate constants than a preset cutoff. Our cutoff ranges from 10 s^{-1} to 10 ps^{-1}, as explained in the caption to Figure 4.

By inspecting Figure 4, we find that there are characteristic distances (in multidimensional configuration space) related to intrametabasin and intermetabasin transitions. There is a shortage of fast transitions with big steps in terms of the Euclidean norm. On the other hand, extending the sampling to slower and slower rates does not change the characteristic distances but increases the observed number of transitions in a manner that only modifies the variance around the most probable values of the displacement in multidimensional space. Interestingly, the relative probabilities of intramacrostate transitions are almost preserved in an all-to-all connection model (top curve, Figure 4b), where each state is linked with all the rest, as would be assumed in a random energy model.

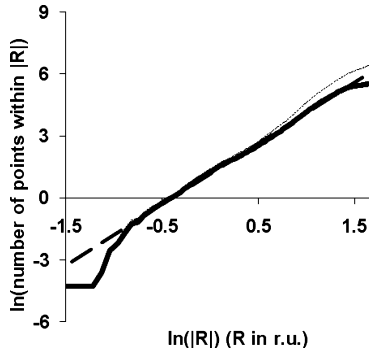

Figure 5. Evaluation of the correlation fractal dimension of the network of potential energy minima of the sampled MB and its neighbors, based on the slope of the logarithm of the number of ISs found within a specific distance |**R**| from a reference IS in the 3 × 641 dimensional configuration space of the system, averaged over all reference ISs, with respect to the logarithm of |**R**|. The short- dashed line includes all possible pairs, irrespective of whether they are directly connected or not; the solid line corresponds only to pairs that are directly connected by a transition sampled by our method. The correlation fractal dimension in both cases is slightly lower than 3 (∼2.95), as calculated from the slope of the linear fit shown with the long-dashed line.

From Figure 5 it is also evident that the configuration space can only be filled with ISs extremely sparsely, since, as one should expect, the accessible part of the configurational space is exponentially smaller than the volume of the configuration space that would be accessible to an ideal gas. This is, of course, related to the repulsive part of the excess free energy of the system. Indeed, by analyzing the network of potential energy minima in the 3 × 641 dimensional space, we estimated a fractal dimension of approximately 2.7 (±0.5), both for the case where we account only for pairs of ISs that are connected directly by our sampling scheme and in the case where we include all possible pairs, irrespective of whether we have found a direct connection between them. The evaluation of the correlation fractal dimension[60] is based on the estimation of the slope of the logarithm of the number of IS points found within a hypersphere of radius R centered at any IS with respect to the logarithm of that radius, as shown in Figure 5.

In order to investigate the degree of localization in the motions leading the system from one basin to another, we evaluated the participation ratio. This has been introduced as a tool for the investigation of the localization of normal mode vibrations around the ISs of glassy systems.[61–63] For each pair of ISs connected via a direct transition, we define the participation ratio as in eq 13:[61,63]

$$P_{\alpha\beta} = \frac{[\sum_{i=1}^{N} (\mathbf{r}_{\alpha\beta}^{i})^2]^2}{N \sum_{i=1}^{N} (\mathbf{r}_{\alpha\beta}^{i})^4} \qquad (13)$$

where $\mathbf{r}_{\alpha\beta}^{i}$ is the three-dimensional displacement vector of atom i, pointing from its position in IS α to its position in IS β. $p_{\alpha\beta}$ should be close to unity if all atoms contribute roughly equally to the multidimensional vector ($\mathbf{r}_{\alpha\beta}^{1}$, ..., $\mathbf{r}_{\alpha\beta}^{i}$, ..., $\mathbf{r}_{\alpha\beta}^{N}$), whereas it should be small for localized displacements. In accordance with the work of Nagel, Grest, and Rahman,[62] we define as localized a displacement vector if $Np_{\alpha\beta}$ is less than $(N)^{1/2}$, that is, in our case, 25.3. By analyzing our results, we found that, on average, $Np_{\alpha\beta} \sim 40$, indicating a collective nature in each of the underlying transitions. As one would expect, there is a correlation between the length traversed by the transition in configuration space and the level of cooperativity. In Figure 6 we plot a histogram of the number of transitions explored as a function of the Euclidean distance traversed in 3 × 641-dimensional configuration space and the participation ratio. There is a clear correlation between the cooperativity and the length traversed. Low values of the participation ratio are only found in transitions traversing a small Euclidean distance. Most of the transitions explored are observed at a characteristic distance around 12 Å with. $Np_{\alpha\beta} \sim 40$. However, we have sampled intrametabasin transitions with $Np_{\alpha\beta}$ more than 100.

Conclusions

In this work we have proposed a methodology for the improvement of the dynamical sampling of atomistic simulations of glassy materials via temperature acceleration. The proposed approach combines a number of different methods: (a) TAD,[12–14] (b) the multiple histogram reweighting method of Ferrenberg and Swendsen,[18] (c) the dynamical extension of multiple histogram reweighting by Nieto-Draghi et al.,[15] and (d) hazard plot analysis.[64,20] It has been especially designed to address the sampling difficulties present in atomistic simulations of glass-forming materials in the vicinity of the glass transition temperature T_g. In general, it can also be applied with minimal modification to a variety of systems provided that the overall dynamics of the systems can be decomposed into fast processes and slow processes governed by Poisson process statistics. In the specific case of glass-forming materials, this separation of time scales is provided via the idea of ISs. The proposed methodology is highly parallelizable and allows the temperature acceleration of the dynamics upon the assumption of Poisson statistics by histogram reweighting of appropriately constructed ensembles of trajectories, providing optimal sampling toward neighboring MBs at small computational cost over time scales inaccessible to classical MD simulations.

The new, temperature-accelerated method offers optimal sampling of the extremely slow transitions with rate constants significantly slower than those that can be evaluated by brute force MD. Its implementation is connected with the parallel method described in previous work.[42] Employing the proposed method in a MB, we identified and evaluated transition rate constants inaccessible to brute force MD. Our ability to evaluate very slow transitions gives us the unique possibility to obtain transition rate constants from and toward any basin of our selected MB. It is of particular importance that, once we obtain those transition rate constants from and toward any basin, our system becomes, by construction, *ergodic* within our preselected MB.

By analyzing the resulting network of interconnected "basins" in terms of the Euclidean space spanned by the potential energy minima, we found that there are characteristic distances related to intrametabasin and intermetabasin transitions. Fast transitions associated with big strides, in terms of the Euclidean norm in configuration space, are absent. On the other hand, extending the sampling to slower and slower rates does not change the characteristic Euclidean distances traversed but increases the observed number of transitions in a manner that only sharpens the distribution around the most probable values. Interestingly, the relative probability of intramacrostate displacements is almost preserved in an all-to-all interaction model where each state is linked with all the rest, as a random energy model would assume.

In order to investigate the localization of the sampled transitions in the multidimensional configurational space within the MB, we evaluated the participation ratio for each of the

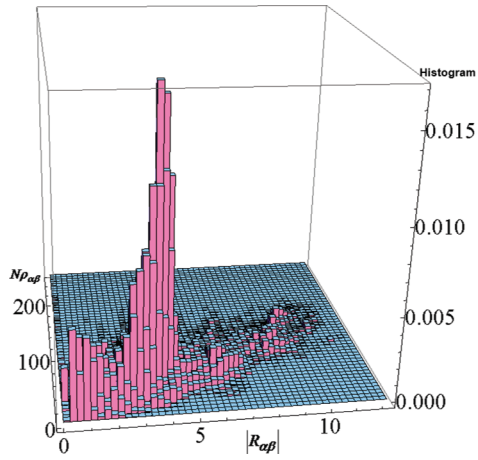

Figure 6. Two-dimensional histogram of inter- and intrametabasin transitions explored over the sampling of four MBs as a function of the Euclidean distance $R_{\alpha\beta}$ (in r.u.) traversed between ISs in the 3×641-dimensional configuration space of the system, and of the participation $Np_{\alpha\beta}$. A clear correlation is seen between the cooperativity and the distance traversed by the explored transitions.

51207 sampled transitions. We found that most of the transitions sampled in our calculations are nonlocal; this is especially true of the transitions that lead out of our MB. We also calculated the fractal dimension of the set of ISs in the MB, which was estimated to be approximately 3.

The ability to simulate for longer times in an efficient parallel manner allowed us to sample features of the potential energy landscape that could not have been seen from ordinary sampling schemes, "mapping out" the wide range of rate constants present in the vicinity of the configuration-space region explored by our dynamical importance sampling. We have shown that there is a characteristic time scale (see Figure 3) associated with the dynamical importance sampling whereby an MB is defined (i.e., it is more probable to find in the surrounding landscape rate constants commensurate with the inverse residence time in the MB). In addition, however, there is also an underlying power-law distribution of slower rate constants (that is, an exponential tail of higher barrier heights) that extends to extremely infrequent phenomena. This seems to be an intrinsic feature of the multidimensional potential energy landscape of glass-forming systems.

Additionally, the evaluation of a correlation fractal dimension of the potential energy minima "maps out" the fractal nature of the underlying network of transitions, revealing a wide range of length scales related to the structural relaxation process. Both wide ranges, of time and length scales, are known to be immediately linked to the nature of the diffusion process,[65] leading to anomalous diffusion (in our case subdiffusion).

Finally, we have shown that (a) transitions spanning longer and longer distances in configuration space are immediately related to collective rearrangements (i.e., the increase of the Euclidean norm of atomic displacements is almost proportional to the increase of the participation ratio; see Figure 6) mainly because of the formation of chain-like structures (Figure 7), and (b) collective transitions of increasing "chain length" are related to intermetabasin transitions, whereas intrametabasin transitions are related to isolated cage-breaking events.[66] In Figure 7, a series of atomic displacement vector fields is presented for characteristic transitions with increasing Euclidean norm and complexity. Figure 7 has been prepared with the help of Jmol, an open-source Java viewer for chemical structures in 3D available from http://www.jmol.org/. Initially, for small values of the Euclidean norm, single cage breaking events are observed (Figure 7a). Then, as the Euclidean norm increases, several events are observed in the same transition (Figure 7b). As the Euclidean norm further increases, and we deal mainly with

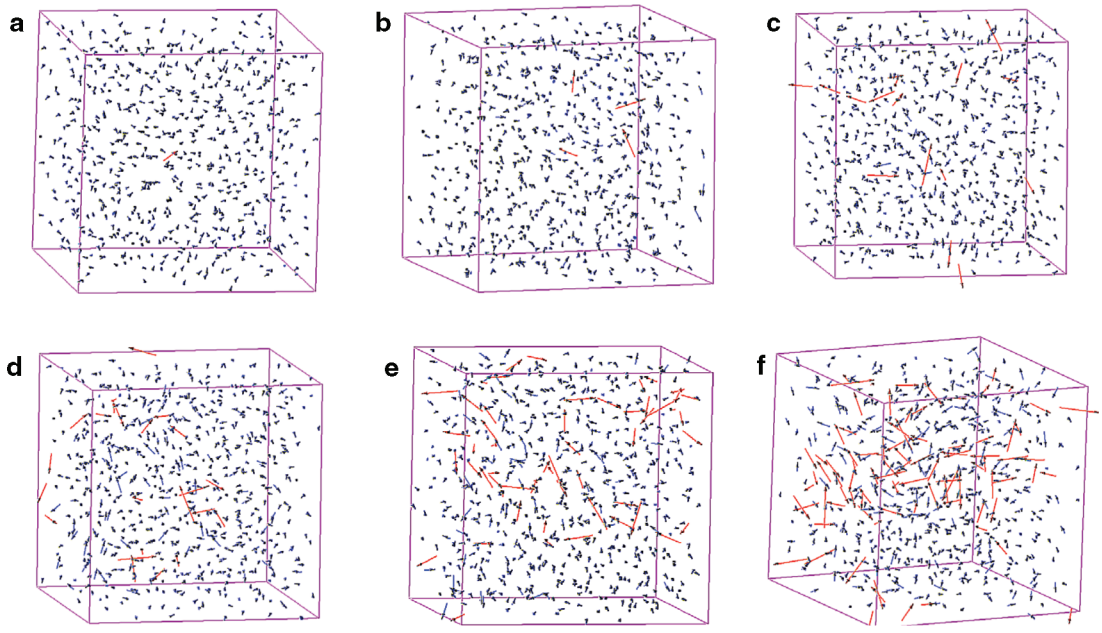

Figure 7. Displacement vectors for each one of the atoms in the system for specific transitions with different Euclidean norms $|\mathbf{R}|$: (a) Equal to 1.7 in r.u. (5.8 Å). (b) Equal to 3.78 in r.u. At this distance, we start observing more than one cage breaking events within the simulation box. (c) Equal to 5.11 in r.u. From this point on, chain formation is evident; based on our analysis, no transition with $|\mathbf{R}| > 5.11$ (in r.u.) is observed without the formation of at least one chain. From this point on, we also deal almost entirely with intermetabasin transitions. (d) Equal to 7.04 in r.u. From this point on, the formation of more than one chains looks probable. (e) Equal to 7.94 in r.u. At this point there is extended formation of several interlinked chains. (f) Equal to 7.94 in r.u. At this point, there is extended formation of several chains, and the size of the individual displacement vectors has increased significantly. In all figures, the red color corresponds to the atom(s) that have moved by more than ~0.6 in r.u. (2 Å). Each box has been centered at the atom with the largest displacement vector for the specific transition.

intermetabasin transitions, formation of chains of atoms moving into each other's position start to appear. With further increase of the Euclidean norm, we reach a point where several such chains span the system, but still a significant part of the system remains relatively immobile. Our observation of a collective nature in displacements is in accordance with the "Stringlike Cooperative Motion" demonstrated by the work[67] of Donati et al. In their work, by analyzing the van Hove correlation function produced via MD simulation for the same model system, Donati et al. showed that there is a fraction of mobile particles that at a characteristic time replace each other, executing a Stringlike Cooperative Motion.

Acknowledgment. This paper is part of the 03ED375 research project, implemented within the framework of the "Reinforcement Programme of Human Research Manpower" (PENED) and cofinanced by National and Community Funds (20% from the Greek Ministry of Development-General Secretariat of Research and Technology and 80% from E.U.-European Social Fund). The authors would like to thank Dr. Loukas Peristeras for his contribution in the development of the parallel code. G.C.B. also would like to thank Dr. Astero Provata for helpful discussions on fractals. This work was carried out under the HPC-EUROPA project (RII3-CT-2003-506079), with the support of the European Community - Research Infrastructure Action under the FP6 "Structuring the European Research Area" Program.

References and Notes

(1) Moore, G. E. *Electronics* **1965**, *38*, 114.
(2) Alder, B. J.; Wainwright, T. E. *J. Chem. Phys.* **1959**, *31*, 459.
(3) Metropolis, N.; Rosenbluth, A. W.; Rosenbluth, M. N.; Teller, A. H.; Teller, E. *J. Chem. Phys.* **1953**, *21*, 1087.
(4) Panagiotopoulos, A. Z. *Mol. Phys.* **1987**, *61*, 813.
(5) Siepmann, J. I.; Frenkel, D. *Mol. Phys.* **1992**, *75*, 59.
(6) Nose, S. *Mol. Phys.* **1984**, *52*, 255.
(7) Ciccotti, G.; Ryckaert, J. P. *Comput. Phys. Rep.* **1986**, *4*, 345.
(8) Streett, W. B.; Tildesley, D. J.; Saville, G. *Mol. Phys.* **1978**, *35*, 639.
(9) Evans, D. J.; Cohen, E. G. D.; Morriss, G. P. *Phys. Rev. Lett.* **1993**, *71*, 2401.
(10) Jarzynski, C. *Phys. Rev. Lett.* **1997**, *78*, 2690.
(11) Schöll-Paschinger, E.; Dellago, C. *J. Chem. Phys.* **2006**, *125*, 054105.
(12) Sorensen, M.; Voter, A. F. *J. Chem. Phys.* **2000**, *112*, 9959.
(13) Montalenti, F.; Voter, A. F. *Phys. Status Solidi B: Basic Res.* **2001**, *226*, 1.
(14) Montalenti, F.; Voter, A. F. *J. Chem. Phys.* **2002**, *116*, 4819.
(15) Nieto-Draghi, C.; Perez-Pellitero, J.; Avalos, J. B. *Phys. Rev. Lett.* **2005**, *95*, 040603.
(16) Rosso, L.; Tuckerman, M. E. *Mol. Simul.* **2002**, *28*, 91.
(17) Zuckerman, D. M.; Woolf, T. B. *Phys. Rev. E* **2000**, *63*, 016702.
(18) Ferrenberg, A. M.; Swendsen, R. H. *Phys. Rev. Lett.* **1989**, *63*, 1195.
(19) Helfand, E. *J. Chem. Phys.* **1978**, *69*, 1010.
(20) Helfand, E.; Wasserman, Z. R.; Weber, T. A. *Macromolecules* **1980**, *13*, 526.
(21) Stillinger, F. H.; Weber, T. A. *Phys. Rev. A* **1982**, *25*, 978.
(22) Heuer, A. *J. Phys.: Condens. Matter* **2008**, *20*, 373101.
(23) Angell, C. A. *J. Non-Cryst. Solids* **1988**, *102*, 205.
(24) Dawson, K. A.; Foffi, G.; Sciortino, F.; Tartaglia, P.; Zaccarelli, E. *J. Phys.: Condens. Matter* **2001**, *13*, 9113.
(25) Boulougouris, G. C.; Frenkel, D. *J. Chem. Phys.* **2005**, *122*, 244106.
(26) Theodorou, D. N.; Suter, U. W. *Macromolecules* **1985**, *18*, 1467.
(27) Souza, V. K. d.; Wales, D. J. *J. Chem. Phys.* **2009**, *130*, 194508.
(28) Souza, V. K. d.; Wales, D. J. *J. Chem. Phys.* **2008**, *129*, 164507.
(29) Middleton, T. F.; Wales, D. J. *J. Chem. Phys.* **2004**, *120*, 8134.
(30) Calvo, F.; Bogdan, T. V.; Souza, V. K. d.; Wales, D. J. *J. Chem. Phys.* **2007**, *127*, 044508.
(31) Tsalikis, D. G.; Lempesis, N.; Boulougouris, G. C.; Theodorou, D. N. *J. Phys. Chem. B* **2008**, *112*, 10619.
(32) Tsalikis, D. G.; Lempesis, N.; Boulougouris, G. C.; Theodorou, D. N. *J. Phys. Chem. B* **2008**, *112*, 10628.
(33) Boulougouris, G. C.; Theodorou, D. N. *J. Chem. Phys.* **2009**, *130*, 044905.
(34) Boulougouris, G. C.; Theodorou, D. N. *J. Chem. Phys.* **2007**, *127*, 084903.
(35) Henkelman, G.; Jónsson, H. *J. Chem. Phys.* **1999**, *111*, 7010.
(36) Munro, L. J.; Wales, D. J. *Faraday Discuss.* **1997**, *106*, 409.
(37) Munro, L.; Wales, D. *Phys. Rev. B* **1999**, *59*, 3969.
(38) Barkema, G. T.; Mousseau, N. *Phys. Rev. Lett.* **1996**, *77*, 4358.
(39) Bolhuis, P. G.; Chandler, D.; Dellago, C.; Geissler, P. L. *Annu. Rev. Phys. Chem.* **2002**, *53*, 291.
(40) Bolhuis, P. G.; Dellago, C.; Chandler, D. *Faraday Discuss.* **1998**, *110*, 421.
(41) Wales, D. J. *Mol. Phys.* **2002**, *100*, 3285.
(42) Tsalikis, D. G.; Lempesis, N.; Boulougouris, G. C.; Theodorou, D. N. *J. Chem. Theory Comput.* **2010**, *6*, 1307.
(43) Pratt, L. R. *J. Chem. Phys.* **1986**, *9*, 5045.
(44) Dellago, C.; Bolhuis, P. G.; Chandler, D. *J. Chem. Phys.* **1999**, *110*, 6617.
(45) Abrams, J. B.; Rosso, L.; Tuckerman, M. E. *J. Chem. Phys.* **2006**, *125*, 074115.
(46) Swendsen, R. H.; Wang, J. S. *Phys. Rev. Lett.* **1986**, *57*, 2607.
(47) Frenkel, D.; Smit, B. Free Energy Calculation In *Understanding Molecular Simulation*; 2nd ed.; Academic Press: New York, 2002; pp 167.
(48) Appignanesi, G. A.; Fris, J. A. R.; Montani, R. A.; Kob, W. *Phys. Rev. Lett.* **2006**, *96*, 4.
(49) Doliwa, B.; Heuer, A. *Phys. Rev. E* **2003**, *67*, 030501.
(50) Buechner, S.; Heuer, A. *Phys. Rev. Lett.* **2000**, *84*, 2168.
(51) Denny, R. A.; Reichman, D. R.; Bouchaud, J. P. *Phys. Rev. Lett.* **2003**, *90*, 025503.
(52) Mauro, J. C.; Loucks, R. J.; Gupta, P. K. *J. Phys. Chem. A* **2007**, *111*, 7957.
(53) Heuer, A. *J. Phys.: Condens. Matter* **2008**, *20*, 373101.
(54) Kob, W.; Andersen, H. C. *Phys. Rev. Lett.* **1994**, *73*, 1376.
(55) Kushima, A.; Lin, X.; Li, J.; Eapen, J.; Mauro, J. C.; Qian, X. F.; Diep, P.; Yip, S. *J. Chem. Phys.* **2009**, *130*, 224504.
(56) Kob, W. *Phys. Rev. E.* **1995**, *51*, 4626.
(57) Kob, W.; Andersen, H. C. *Phys. Rev. E* **1995**, *51*, 4626.
(58) Kob, W.; Andersen, H. C. *Phys. Rev. E* **1995**, *52*, 4134.
(59) Shell, M. S.; Debenedetti, P. G.; Panagiotopoulos, A. Z. *Fluid Phase Equilib.* **2006**, *241*, 147.
(60) Mandelbrot, B. *Fractals - Form, Chance and Dimension*; W. H. Freeman: San Francisco, 1977.
(61) Bell, R. J.; Dean, P.; Hibbins-Butler, D. C. *J. Phys. C.* **1970**, *3*, 2111.
(62) Nagel, S. R.; Grest, G. S.; Rahman, A. *Phys. Rev. Lett.* **1984**, *53*, 368.
(63) Goldenberg, C.; Tanguy, A.; Barrat, J.-L. *Eur. Phys. Lett.* **2007**, *80*, 16003.
(64) Helfand, E. *J. Chem. Phys.* **1978**, *69*, 1010.
(65) Metzler, R.; Klafter, J. *Phys. Rep.* **2000**, *339*, 1.
(66) Vollmayr-Lee, K. *J. Chem. Phys.* **2004**, *121*, 4781.
(67) Donati, C.; Douglas, J. F.; Kob, W.; Plimpton, S. J.; Poole, P. H.; Glotzer, S. C. *Phys. Rev. Lett.* **1998**, *80*, 2338.

JP908975D